Iranian Polymer Journal
20 (6), 2011, 523-533

Available online at: http://journal.ippi.ac.ir

Direct Condensation of *d,l*- and *l*-Lactic acids: Effect of $AlCl_3$ Catalyst on Microstructural Arrangements of Homopolymers and Copolymers

Selvaraj Nagarajan[1], John Tsibouklis[2], and Boreddy Siva Rami Reddy[1*]

(1) Industrial Chemistry Laboratory, Central Leather Research Institute, Chennai-600 020, India
(2) Biomaterials and Drug Delivery Research Group, School of Pharmacy and Biomedical Sciences, University of Portsmouth, Portsmouth, Hampshire PO1 2DT, UK

Received 24 September 2010; accepted 23 May 2011

ABSTRACT

The effect of $AlCl_3$ as a catalyst in direct condensation of homopolymerization and copolymerization of (*rac* and *l*)-lactic acid was studied. The morphological effect of dimer formation via racemization during polymerization with respect to time and catalyst concentration was investigated at 180°C under vacuum conditions (176 mmHg). The sequence distribution of triads and hexads was analyzed using ^{13}C NMR spectroscopy. A combination of Avrami and Ozawa equations for mathematical modelling of the non-isothermal crystallization kinetics of the synthesized poly(*d,l*-lactic acid) produced consistent results with the experimental data under these conditions. It is shown that $AlCl_3$ promotes racemization which leads to formation of ill-defined polymers, as demonstrated by determinations of molecular weight distribution ($\overline{M}_n$ < 5279 g/mol, PDI = 1.4-3), optical purity (91.67% - 99.36%) and melting temperature (143-155°C). The activation energy for crystal growth during the cooling of molten samples of poly(*d,l*-lactic acid), as determined by Kissinger method, is found to be 45 kcal per mol. In this respect, the microstructural effect of copolymers on their thermal behaviour is discussed.

Key Words:

activation energy;
amorphous;
crystallization;
esterification;
microstructure.

INTRODUCTION

The biodegradability and bioabsorption of polylactic acid (PLA) are favourable properties which make this polymer as a versatile component of biomedical products [1-3]. The properties of PLA may be refined according to the demands of each application by altering the conditions of the polymerization reaction and/or by copolymerization [4-7]. The biomedically relevant properties of bioabsorption and biodegradation are highly sensitive to the degree of crystallinity, due to dominant amorphous regions of the semi-crystalline PLA structure hydrate relative to crystalline regions which are determined by the microstructural arrangement around the chiral-carbon atoms [8-11].

In general, pure *d*- or *l*-lactic acid and *l*- or *d*-lactides yield highly crystalline isotactic PLA, whereas *meso*-lactides or *d,l*-lactic acid

(*) To whom correspondence to be addressed.
E-mail: bsrredy.clri@gmail.com

produce atactic PLA. Chabot et al. [12] investigated the stereosensitivity of the carbonyl group as a function of lactide-comonomer composition and reported the effects of changing microstructural arrangement of PLA on the thermal properties of the material. Stayshich et al. [13] reported the synthesis of lactic acid and glycolic acid copolymers and recorded the NMR chemical shifts of hexad sequences. Coats et al. [14] reported that the syndiotatic PLA has lower melting point than isotatic and atactic PLAs.

The microstructural arrangements of the polymer and the molecular weight influence the thermal behaviour. Towards the industrial-scale production of high molecular weight PLA polymers, bulk, solution and solid condensation methods, and other polymerization techniques have been attempted, with a limited success [15,16]. The structurally designed low molecular weight PLA polymers with high optical purity provide better control of biomedically relevant properties such as cell adhesion, bioabsorbtion and/or biodegradation [8-11]. Lewis acids such as $ZnCl_2$, Al(acac), Sn(II)Oct, dibutyltin dilaurate (DBTL) and Sb_2O_3 were used to examine racemization process which depends on catalyst concentration and polymerization temperature [17].

This study involved the optimization of the conditions for the effect of microstructural arrangements on the thermal behaviour of copolymers synthesized from *d,l*- and *l*-lactic acids influenced by weak Lewis acid catalyst ($AlCl_3$). Several low molecular weight congeners of this polymer have been prepared by bulk utilizing $AlCl_3$ as a catalyst.

EXPERIMENTAL

Materials

Aqueous solutions of *l*- and *d,l*-lactic acids (LA; 90%) were obtained from Sigma (USA) or from S.D. Fine-Chem, India. Anhydrous $AlCl_3$ was purchased from Merck, Germany. Phosphate buffer saline was procured from Hi-media India. Chloroform, hexane and diethylether were purchased from Rankem, India. All materials were used without further purification.

Polycondensation

To a three-necked round-bottom flask (250 mL), fitted with a funnel and a condenser which was connected to an extended vacuum system via a cool trap and a calcium chloride tube was introduced predetermined amounts (92-100% *l*-lactic acid, Table 1) of aqueous solutions of the monomer and/or the comonomers. To remove water, the temperature of the reaction was maintained at 100±5°C for 3 h. Then, a specified amount of $AlCl_3$ (0.4-0.8% of total monomers weight) was added and the temperature was raised slowly to 180±5°C. The end of the reaction was signaled by the onset of depolymerization as indicated by the deposition of sublimed dimers on the inner wall of the condenser (*ca.*, 10 h). After being cooled to room temperature the mixture was washed with diethylether (3×25 mL) and

Table 1. Reaction conditions effects on polymer characteristics of bulk polymerization of LA in the presence of $AlCl_3$.

Entry No.	*l*-Lactic acid (%)	*d,l*-Lactic acid (%)	Catalyst (wt%)	Temperature (°C)	Time (h)	Dimer (wt%)	$\overline{M}_n$ (g/mol)	PDI	OP (%)
1	100	-	0.8	170	25.00	5.00	4533	1.8	-
2	100	-	0.8	170	19.00	8.00	4165	1.4	84
3	100	-	0.8	200	14.00	8.20	3377	1.5	-
4	-	100	0.8	170	12.50	1.25	3994	1.3	90
5	-	100	0.8	180	18.00	1.60	5233	1.8	-
6	80	20	0.4	180	13.00	2.00	5279	1.7	92
7	84	16	0.4	180	19.50	9.00	3561	1.7	96
8	88	12	0.4	180	15.00	3.00	4993	1.3	90
9	92	8	0.4	200	18.50	5.50	1415	3.0	93

$\overline{M}_n$: Number average molecular weight and OP: optical purity = $[\alpha]_D^{27}$ *l*-156 ×100.

dissolved in chloroform (10 mL). The polymeric product was isolated by dropwise addition of the chloroform solution into hexane (500 mL). The polymeric product was isolated by filtering and drying at 60°C for 24 h.

NMR Analysis

^{13}C NMR spectra (TMS, $CDCl_3$) were recorded using a Jeol ECA-500 MHz spectrometer, Japan. NMR Spectra were recorded by performing 4000 scans, pulse delay of 1.2 s, acquisition time of 1.6672, data point of 65536 s and pulse width of 10.2 μs.

Gel Permeation Chromatography

The molecular weight distribution ($\overline{M}_n/\overline{M}_w$) of polymers was determined by a Jasco gel permeation chromatography (MX2080-31, USA) using mixed-C column, RI detector; tetrahydrofuran (THF) 1 mL min^{-1} at 30°C. Polystyrene standards were used to calibrate the molecular weights.

Optical Microscope

Microscopic study was performed by a hot-stage polarizing optical microscope (Olympus BX50, USA; Linkam THM heating stage (UK), and TM90 temperature programmer). A sample was heated at the rate of 10°C per minute up to 170°C, held isothermally for 1 min before cooling at the rate of 5°C per minute to room temperature.

Differential Scanning Calorimeter

DSC experiments (TA-Q200, aluminium pan, 5 ± 0.5 mg) were performed under nitrogen atmosphere.

Polarimeter

The specific rotation $[\alpha]_D^{26}$ of each sample was measured (589 nm) using an Autopol II-30018, Rudolph research analytical instrument.

RESULTS AND DISCUSSION

A two-stage bulk polycondensation of lactic acid yielded materials with number average molecular weights ≤ 5,300 g/mol, Table 1. The first stage of the reaction involved the removal of water from the monomer and the onset of the second stage was the introduction of the catalyst $AlCl_3$ which showed good miscibility with the monomer at elevated temperatures. An essential component of the experimental setup was the cold trap which collected HCl and/or H_3O^+ formed from the interaction of $AlCl_3$ with traces of residual water and/or water formed during the condensation reaction.

Increasing the proportion of the catalyst or the temperature during the second stage of the reaction appears to promote depolymerization, as it is indicated by the increased amounts of dimer (1.25%-9%) formed and by the corresponding broadening of the molecular weight distribution (Table 1). The dimers condensed on the walls of the condenser during vacuum distillation. The depolymerization was not accompanied by discoloration, which was evident by optical purity of 91% to 99.8% range.

^{13}C NMR Spectroscopy

The ^{13}C NMR spectra of LPLA and RPLA polymers (Figure 1c) of similar molecular weight and PDI are taken for comparison (entries 2 and 4) exhibit resonances at 16.71, 69.08 and 169.69 ppm which are attributed to their respective CH, CH_3 and COO functionalities. RPLA exhibits a signal due to the carboxylic acid end groups at 173.3 ppm and multiple carbonyl environments at 169.3-169.9 ppm, consistent with racemization phenomenon and may indicate the formation of some cyclic structures. The sequence distributions of carbonyl and methyl regions were compared with the previously reported theoretical Bernollian statistical analysis of hexad and tetrads.

The individual shifts corresponding to the carbonyl and methyl regions are attributed to the stereochemical effect. The shifts around 169.15-169.45 ppm represent iiisi, iisii, sisii, sisis, iisis and isiii hexads. The shifts around 169.45-169.7 ppm represent iiiii, iiiis, siiii and siiis. The chemical shift at 169.05-169.15 ppm is assigned to isisi.

The shift intensities vary with respect to monomer concentration, sequence distribution and/or racemization effect [18-22]. From the sequence distributions data obtained in our work, chemical shifts around 169.05-169.15 ppm, corresponding to syndiotactic hexad, are absent and a new high intensity shift at 169.6-169.7 ppm is observed in the isotactic region.

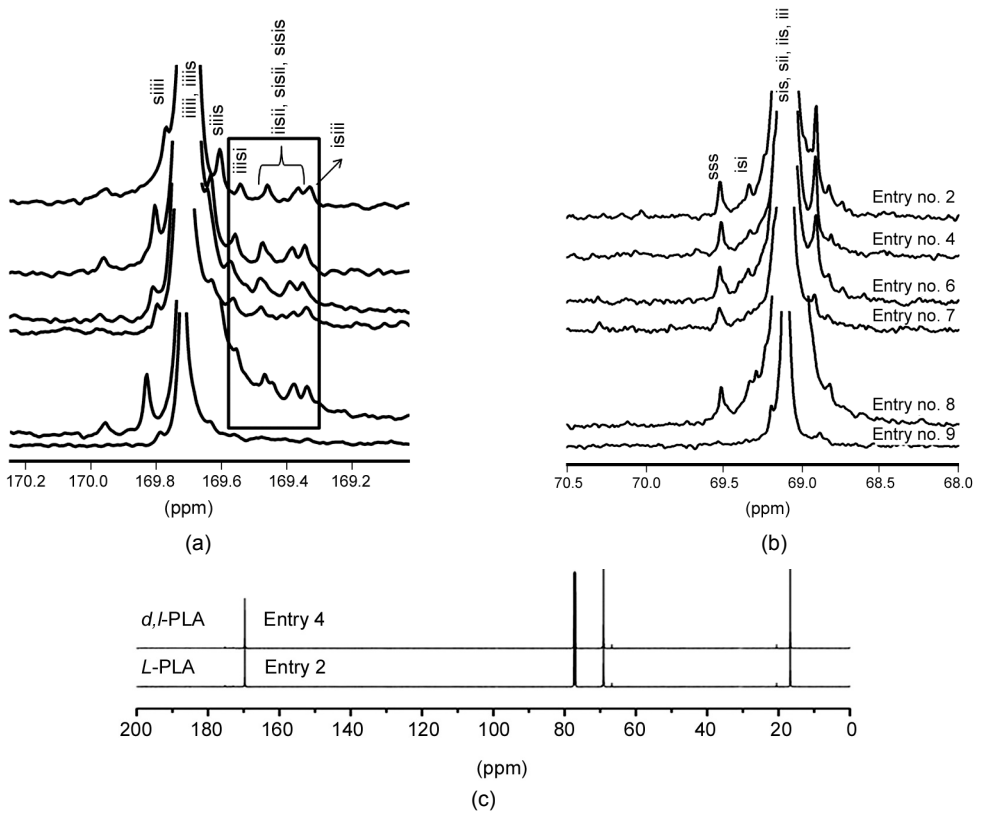

Figure 1. ^{13}C NMR Spectra of: (a) hexad sequences (entries of Table 2), (b) tetrad sequences (entries of Table 2) of *l*- and *d,l*-stereocopolymers, and (c) *d,l*- PLA and *l*-PLA (entries of Table 1).

Some of the very low intensity shifts around 169.15-169.50 are observed in the atactic region. Six different compositions of *d,l*-PLA and *l*-PLA were prepared. There was no significant difference in the chemical shifts observed in ^{13}C NMR except that small shifts were observed at 169.76 ppm and 169.80 ppm (Figure 1a) which appeared to correspond to siiii hexad sequence.

The integral values of hexad sequence (siiii) increased with increase in the *d,l*-lactic acid monomer concentration (Table 2). The shifts overlapping or very close peak to those of iiiii, iiiis sequences are observed for entry 2. The predominant methyl chemical shift at 69.09 ppm corresponds to iii, iis, sii and sis sequences which is influenced by sss sequence and may disturb the crystallinity of polymeric chains. Minor chemical shift at 69.53 ppm corresponds to tetrad sss sequence. Tetrad sequence

Table 2. Tetrad and hexad percentages of *l*- and *d,l*-stereocopolymers.

En no.	Tetrad intensity (%)					Hexad intensity (%)						Mp (°C)
	ssi	sss $\times10^{-3}$	isi $\times10^{-3}$	iss	sis, iis, sii, iii	siiii $\times10^{-3}$	iiiii, iiiis	siiis $\times10^{-3}$	iiisi $\times10^{-3}$	iisii $\times10^{-3}$	isiii $\times10^{-3}$	
2	-	2.25	1.74	-	99.99	-	99.98	3.49	1.50	2.76	1.13	143
4	-	1.11	1.60	-	99.99	3.96	99.98	5.15	5.15	4.60	1.81	155
6	-	1.68	1.24	-	99.99	1.16	99.97	9.99	6.59	4.32	6.51	-
7	-	1.76	1.91	-	99.99	1.63	99.97	7.05	5.11	8.38	3.90	147
8	-	0.92	2.32	-	99.99	3.14	99.98	2.51	1.72	2.32	1.35	151
9	-	-	990	-	90.09	3.14	90.07	9908	8.11	3.28	1.80	-

Mp : Melting point.

integral values of sss sequence at 69.53 ppm are increased with increase in *l*-lactic acid concentration. The increase in sss sequence may disturb the crystallinity in the polymer chain.

The percentage of tetrad and hexad sequences of methyl and carbonyl groups were calculated from the integral values of polymers and were surprisingly found to be more than 90%. In majority of sequences, 99.98% of peak intensity values were observed for isotactic chains. Nicolas et al. [23] reported aluminium alkoxide initiated poly(*d,l*-lactide) showed only 93.5% of tetrads representing iii, iis, sii, sis and ssi sequences. The strong Lewis acids, e.g., $ZnCl_2$, Al(acac), Sn(II)Oct, dibutyltin dilaurate (DBTL) and Sb_2O_3 are responsible for racemization during condensation and yielded racemized product of 33.8, 4.0-6.6, 4.1-4.5, 16.3 and 0.7-3.9 mol%, respectively [17]. Self-condensation of lactic acid using $AlCl_3$ results in 99.99% of tetrads and 99.98% hexads which are dominant for isotactic sequences.

Small changes in the segmental arrangement may be able to change the thermal behaviour of polymeric matrix. The distributions of all monomer compositions were found to display small deviation in

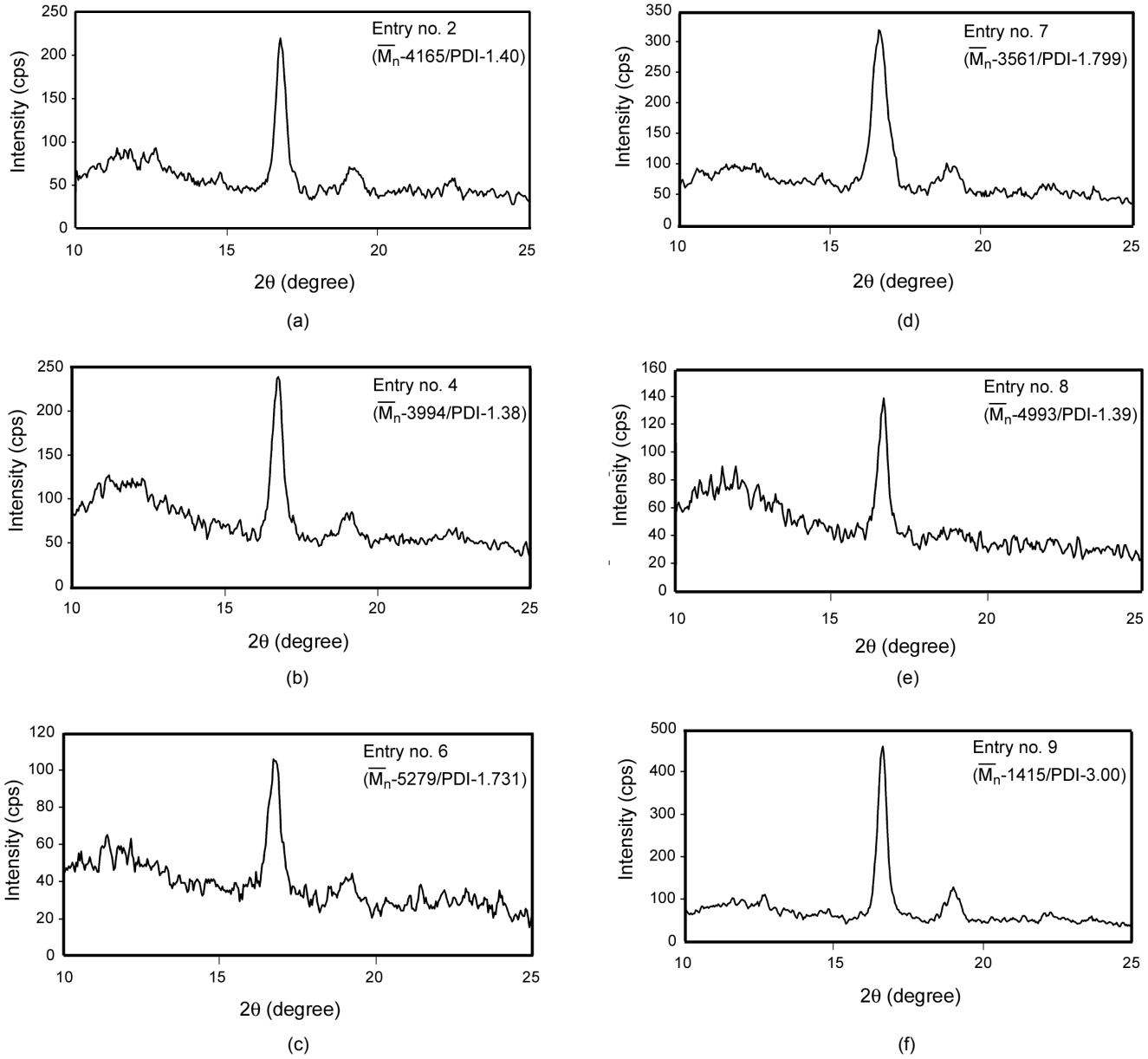

Figure 2. XRD Patterns of various molecular weights PLA.

the chemical shift that may be affecting the crystal growth and melting point of the polymer. The different monomer compositions of $AlCl_3$ catalyzed lactic acid produce predominantly isotactic sequence in the polymer. The lack of a lactonic carbonyl shift (*ca.* 167.6 ppm) is consistent with the absence of appreciable amounts of lactide oligomer in both products.

XRD Spectroscopy

The XRD peaks at 17° (110/200) and at 19° (203) (Figure 2) show that the crystalline component of PLA samples is in its α-form where two chains with 10^3 helical conformations are packed into an orthorhombic unit cell with dimensions a = 10.7 Å, b = 6.45 Å and c (orientation axis) = 27.8 Å [24,25]. The higher crystalline order, displayed in the intensity of XRD features, is indicative of decreasing average molecular weight. Entries 2 and 4 in Figure 2a and 2b, respectively show similar intensities with respect to their molecular weights and molecular weight distributions.

Non-isothermal Crystallization Kinetics

The kinetics of the non-isothermal crystallization of RPLA (entry 4) was investigated by DSC technique as shown in Figure 3. The highest peak crystallization temperature (T_c: 119°C) was observed at a cooling rate of 5°C/min. Crystal growth appears to be influenced by cooling rate, with samples cooled at 1°C/min exhibiting lower crystallinity than those cooled at 3°C/min. At cooling rate of 5°C/min, RPLA exhibited dual crystal peaks between 123°C and 84°C which are not replicated at cooling rates of 3°C/min or 1°C/min.

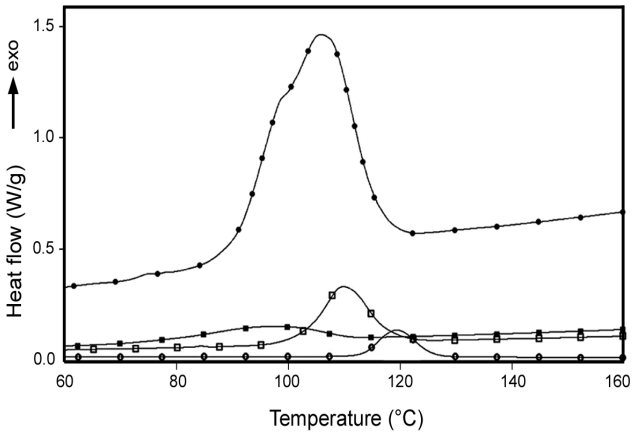

Figure 3. DSC Thermograms of LPLA with a cooling rate of 3°C/min (■) and RPLA under multiple cooling rates of: 1°C/min (○), 3°C/min (□) and 5°C/min (●).

Integration of dH_c/dT (dH_c is enthalpy of crystallization at infinitesimal temperature dT) over a specified range of the DSC thermogram (eqn (1)) yields the relative crystallization (X_t) of RPLA with respect to temperature (T_t): T_{on} = onset point and T_α = end of crystallization as follows:

$$X_t = \frac{\int_{T_{on}}^{T_t} \left(\frac{dH_c}{dT} \right) dt}{\int_{T_{on}}^{T_\alpha} \left(\frac{dH_c}{dT} \right) dt} \quad (1)$$

Data for X_t as a function of RPLA crystallization temperature and as a function of time are presented in Figure 4.

The non-isothermal crystallization of RPLA appears to exhibit the same type of thermal behaviour irrespective of the cooling rate. The non-isothermal crystallization temperature with respect to time has been calculated by eqn (2) as follows:

$$t = \frac{T_0 - T}{\varphi} \quad (2)$$

where,

T_0 = initial temperature,

T = temperature,

t = temperature at crystallization time and,

φ = cooling rate

The ΔH value associated with the cooling rate of 5°C/min was considerably higher than those for cooling rates of 1°C/min or 3°C/min. The crystal growth in RPLA was encouraged by rapid cooling as shown in Table 3.

It is possible that slow cooling rates promote the decomposition of nucleation sites or alternatively encourage thermal decomposition and/or depolymerization which in turn makes impact upon crystal growth [26,27]. The relative degree of crystallinity was evaluated from Avrami expression (eqn (3)) in its logarithmic form (eqn (4)) with estimated values of the exponent n and the rate parameter Z_c obtained using the Jeziorny [28] modification (eqn (5)). This

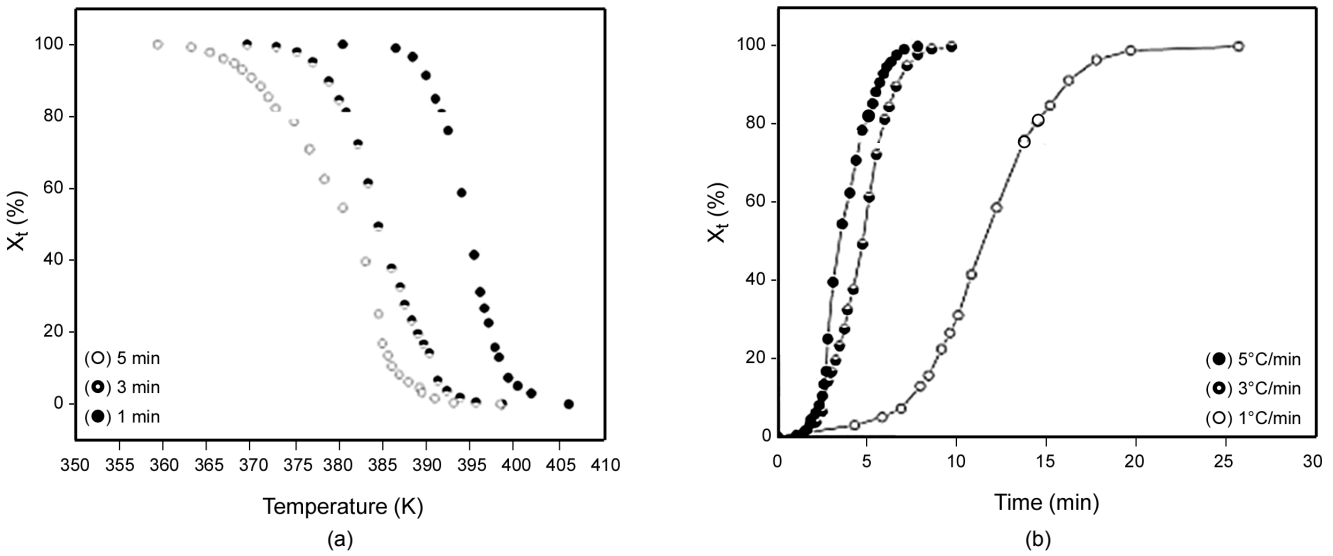

Figure 4. Plots of: (a) X_t vs. temperature and (b) X_t vs. time.

Table 3. The effect of cooling rate on the thermal behaviour of RPLA.

Cooling rate (°C/min)	Z_c	n	$t_{1/2}^*$ (min)
1	0.0179	3.61692	3.87
3	0.4513	3.34587	1.15
5	0.6227	3.71987	1.02

$t_{1/2}^*$ is derived by $t_{1/2} = n(\ln 2/Z_c)^{1/n}$.

allows the mathematical modelling of the effect of the rate of temperature change during non-isothermal crystallization (Table 4).

$$(1-X_t) = \exp(-Z_t t^n) \quad (3)$$

$$\log[-\ln(1-X_t)] = \log Z + n\log t \quad (4)$$

$$\ln Z_c = \frac{\ln Z_t}{\varphi} \quad (5)$$

Plots of *log [-ln(1-X_t)]* versus *log t* are presented in Figure 5. The deviation from linearity shown in Figure 5 may be explained in terms of secondary crystallization and/or the extent of dual spherulite formation at each time interval, as indicated by OMS (Figure 6). Plot variability was considered to be indicative of differences in nucleation mechanism and/or crystal growth during the latter stages of the process.

Values of $n \geq 3.34$ were consistent with the formation of the three dimensional, spherical, RPLA structures visualized by OMS [26-28]. Samples of LPLA, cooled from 160°C at 3°C/min were predominantly non-crystalline at all temperatures range which was due to the decomposition of crystals in molten stage. In RPLA, primary crystallization was completed within 8.30 min, and that of secondary crystallization within a further 15 min. The growth of

Table 4. The effect of cooling rate on non-isothermal crystallization of RPLA.

Cooling rate (°C/min)	T_{on} (°C)	T_c (°C)	T_α (°C)	ΔH (J/g)
1	105.94	119.45	127.38	52.36
3	95.06	109.79	121.10	51.67
5	84.87	105.79	123.89	189.00

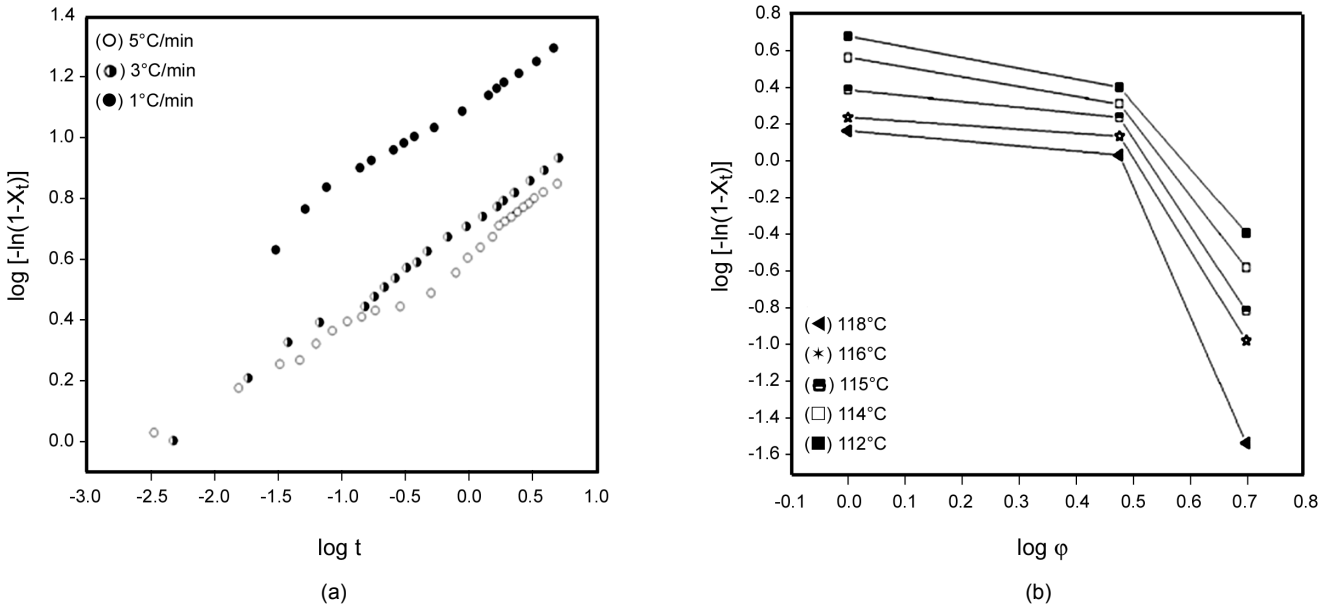

Figure 5. Plots of log [-ln(1-X_t) versus (a) log t and (b) log φ.

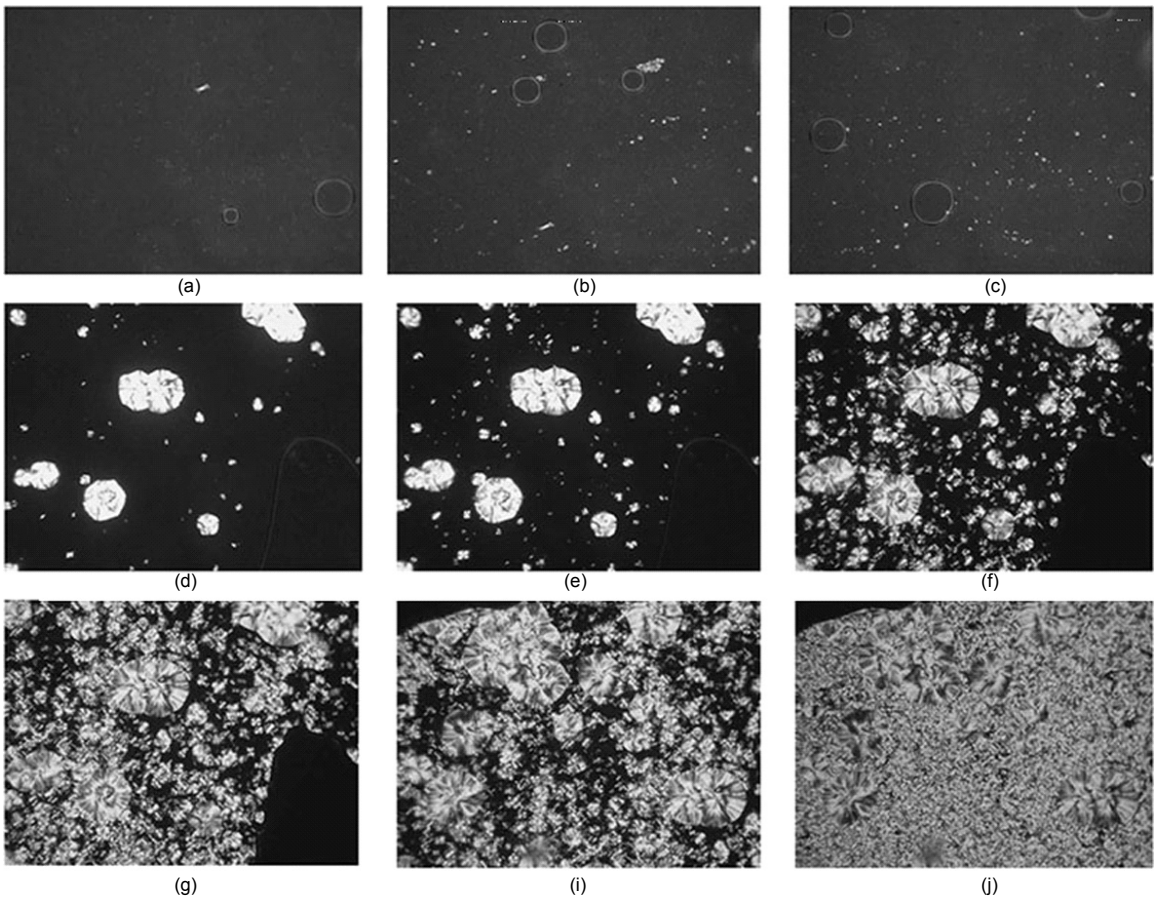

Figure 6. LPLA and RPLA cooled from 150°C at the rate of 5°C/min. (a), (b), and (c) correspond to LPLA after 6 min, 12 min, and 16 min, respectively and (d), (e), (f), (g), (I), and (j) correspond to RPLA after 8.30 min, 8.45 min, 9.00 min, 10.00 min, 11.00 min, and 15.00 min, respectively.

primary and secondary spherulites was evidenced by OMS (Figures 6d-6j). For RPLA, Z_c values increased with increasing the cooling rate, indicating a correspondingly increasing rate of crystal growth. According to the Ozsawa modification of the Avrami equation:

$$X(T) = 1 - \exp\left(-\frac{K(T)}{\varphi^m}\right) \quad (6)$$

$$\log[-\ln(1 - X(T))] = \log K(T) - m \log \varphi \quad (7)$$

where, *X(T)* is a function of temperature and *m* is the Ozsawa exponent denoting nuclei formation, crystal growth and crystal dimension. The plots of *log[-ln(1-X_t)]* versus *log* φ, as shown in Figure 5b are not linear. Hence, *K(t)* cannot be determined using this approach. An alternative approach, proposed by Liu et al. (Mo method) [29,30] combines the Avrami and Ozsawa equations to model relative crystallinity in non-isothermal crystallization in terms of unit crystallization time.

$$\log Z - n \log t = \log K(T) - m \log \varphi \quad (8)$$

$$\log \varphi = \log F(T) - \alpha \log t \quad (9)$$

where, $F(T) = [K(T)/Z]^{1/m}$ represents cooling with respect to unit crystallization time and $\alpha = m/n$. The plots of *log t* versus *log* β were found to be straight lines as shown in Figure 7a. The Mo approach may be considered to provide an appropriate description of the non-isothermal crystallization of RPLA. Values of *F(T)* and α are correspondingly determined from the intercept and slope as presented in Table 5. *F(T)* values were found to increase progressively with increased relative crystallinity though α values were in the range of 1.26 to 1.43.

The Kissinger method allowed the calculation of the activation energy for transport of unit crystal growth related to the free energy barrier for nucleation as follows:

$$\frac{d[\ln(\varphi / T_c^2)]dy}{d(1/T_c)} = \frac{-\Delta E}{R} \quad (10)$$

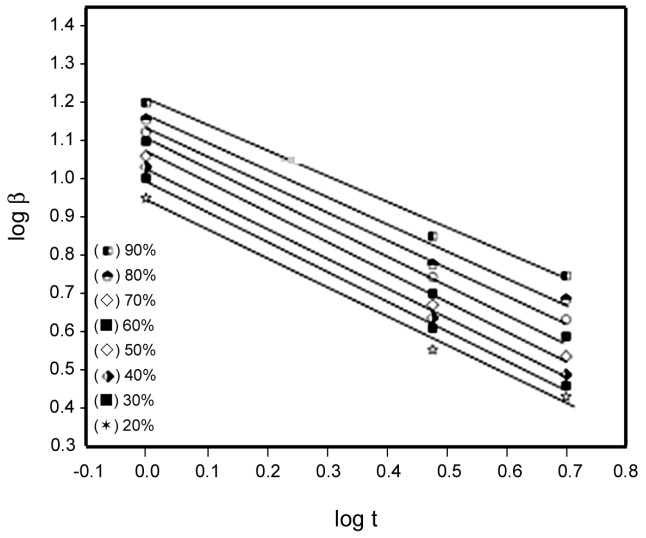

(a)

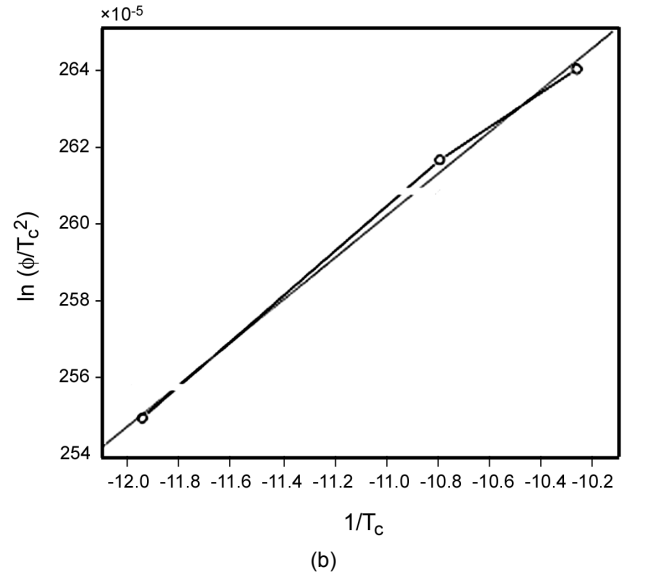

(b)

Figure 7. Plots of: (a) log t vs. log β and (b) $\ln(\phi/T_c^2)$ vs. $1/T_c$.

Table 5. The effect of cooling rate on kinetic parameters characterizing the non-isothermal crystallization of RPLA.

X_t (%)	F(t)	α	ΔH (kcal/mol)
20	1.19320	1.26722	
30	1.23812	1.24348	
40	1.30464	1.26953	
50	1.38094	1.30836	45
70	1.52696	1.36819	
80	1.61096	1.40156	
90	1.71675	1.43344	

where, ΔE is the activation energy (energy barrier), T_c is peak temperature and R is universal gas constant.

A plot of $Ln(\phi/T_c^2)$ versus $1/T_c$ allows the determination of the activation energy ($\Delta E = -2.303R \times$ slope) for the non-isothermal crystallization of RPLA (Figure 7b).

CONCLUSION

The use of $AlCl_3$ catalyst in the polycondensation of lactic acid promotes predominantly isotactic sequence in copolymers with different feed composition of *l*-lactic acid and *d,l*-lactic acid. The optical purity (84% to 96%) and melting temperature (143-155°C) changes were observed with different copolymerization compositions. Melting point of the polymer considerably increases by increasing the composition of *d,l*-lactic acid. Thermal activation energy for crystal growth during the cooling of molten samples of poly(*d,l*-lactic acid) (entry 4) was determined as 45 kcal mol^{-1}.

ACKNOWLEDGEMENT

S.Nagarajan thanks CSIR, New Delhi, for the Senior Research Fellowship and authors acknowledge financial support from DST, New Delhi (No.SR/S1/PC-33/2006).

REFERENCES

1. Ozkoc G, Kemaloglu S, Morphology, biodegradability, mechanical, and thermal properties of nanocomposite films based on PLA and plasticized PLA, *J Appl Polym Sci*, **114**, 2481-2487, 2009.
2. Nampoothiri KM, Nair NR, John RP, An overview of the recent developments in polylactide (PLA) research, *Biores Technol*, **101**, 8493-8501, 2010.
3. Zamiri P, Kuang Y, Sharma U, Ng TF, Busold RH, Rago AP, Core LA, Palasis M, The biocompatibility of rapidly degrading polymeric stents in porcine carotid arteries, *Biomaterials*, **31**, 7847-7855, 2010.
4. Gupta AP, Kumar V, New emerging trends in synthetic biodegradable polymers - polylactide: a critique, *Eur polym J*, **43**, 4053-4074, 2007.
5. Xiong L, He Z, The biological evaluation of the PEG/PLA amphiphilic diblock copolymer, *Polym Plast Technol Eng*, **49**, 1201-1206, 2010.
6. Wang Z-Y, Zhao H-J, Wang Q-F, Ye R-R, Finlow DE, Synthesis of poly(*D,L*-lactic acid) modified by cholic acid via direct melt copolycondensation and its characterization, *J Appl Polym Sci*, **117**, 1405-1415, 2010.
7. Namkajorn M, Petchsuk A, Opaprakasit M, Opaprakasit P, Synthesis and characterizations of degradable aliphatic-aromatic copolyesters from lactic acid, dimethyl terephthalate and diol: effects of diol type and monomer feed ratio, *eXPRESS Polym Let*, **4**, 415-422, 2010.
8. Mihai M, Huneault MA, Favis BD, Crystallinity development in cellular poly(lactic acid) in the presence of supercritical carbon dioxide, *J Appl Polym Sci*, **113**, 2920-2932, 2009.
9. Zhou Q, Xanthos M, Nanoclay and crystallinity effects on the hydrolytic degradation of polylactides, *Polym Deg Stab*, **93**, 1450-1459, 2008.
10. Silva MP, SencadasV, Botelho G, Machado AV, Rolo AG, Rocha JG, Lanceros-Mendez S , α- and γ-PVDF: crystallization kinetics, microstructural variations and thermal behavior, *Mat Chem Phy*, **122**, 87-92, 2010.
11. Nagarajan S, Reddy BSR, Bio-absorbable polymers in implantation: an overview, *J Sci Indus Res*, **68**, 993-1009, 2009.
12. Stayshich RM, Meyer TY, New insights into poly(lactic-co-glycolic acid) microstructure: using repeating sequence copolymers to decipher complex NMR and thermal behavior, *J Am Chem Soc*, **132**, 10920-10934, 2010.
13. Chabot F, Vert M, Chapelle S, Granger P, Configurational structures of lactic acid stereocopolymers as determined by ^{13}C---{^1H} n.m.r., *Polymer*, **24**, 53-59, 1983.
14. Ovitt TM, Coates GW, Stereochemistry of lactide polymerization with chiral catalysts: new opportunities for stereocontrol using polymer exchange mechanism, *J Am Chem Soc*, **124**, 1316-1326, 2002.
15. Li Y, Sun XS, Preparation and characterization of

polymer-inorganic nanocomposites by in situ melt polycondensation of *L*-lactic acid and surface-hydroxylated MgO, *Biomacromolecules*, **11**, 1847-1855, 2010.
16. Sedlarik V, Kucharczyk P, Kasparkova V, Drbohlav J, Salakova A, Saha P, Optimization of the reaction conditions and characterization of *L*-lactic acid direct polycondensation products catalyzed by a non-metal-based compound, *J Appl Polym Sci*, **116**, 1597-1602, 2010.
17. Hiltunen K, Seppala JV, Harkonen M, Effect of catalyst and polymerization conditions on the preparation of low molecular weight lactic acid polymers, *Macromolecules*, **30**, 373-379, 1997.
18. Shyamroy S, Garnaik B, Sivaram S, Structure of poly(*L*-lactic acid)s prepared by the dehydropolycondensation of *L*-lactic acid with organotin catalysts, *J Polym Sci Pol Chem*, **43**, 2164-2177, 2005.
19. Nouailhas H, Li F, Ghzaoui AE, Li S, Coudane J, Influence of racemization on stereocomplex-induced gelation of water-soluble polylactide-poly(ethylene glycol) block copolymers, *J Polym Int*, **59**, 1077-1083, 2010.
20. Belleney J, Wisniewski M, Le Borgne A, Influence of the nature of the ligand on the microstructure of poly *D,L*-lactic acid prepared with organoaluminum initiators, *Euro Polym J*, **40**, 523-530, 2004.
21. Zhao P, Wang QF, Zhong Q, Zhang NW, Ren J, Microstructre and mechanism study of polylactic acid obtained by the copolymerization of *L*-lactide and *D,L*-lactide, *J Appl Polym Sci*, **115**, 2955-2961, 2010.
22. Zhang P, Feng Y, Zhou R, Zhao J, Synthesis and characterization of amphiphilic copolymer acrylic acid-*co*-p-chloromethylstyrene, *J Macromol Sci Pure Appl Chem*, **46**, 32-36, 2009.
23. Spassky N, Wisniewski M, Pluta C, Le Borgne A, High stereoelective polymerization of rac-(*D,L*)-lactide with a chiral Schiff's base/aluminiumalkoxide initiator, *Macromol Chem Phys*, **197**, 2627-2637, 1996.
24. Pan P, Zhu B, Kai W, Dong T, Inoue Y, Polymorphic transition in disordered poly(*L*-lactide) crystals induced by annealing at elevated temperatures, *Macromolecules*, **41**, 4296-4304, 2008.
25. Maillard D, Prud'Homme RE, Differences between crystals obtained in PLLA-rich or PDLA-rich stereocomplex mixtures, *Macromolecules*, **43**, 4006-4010, 2010.
26. Rahman N, Kawai T, Matsuba G, Nishida K, Kanaya T, Watanabe H, Okamoto H, Kato M, Usuki A, Matsuda M, Nakajima K, Honma N, Effect of polylactide stereocomplex on the crystallization behavior of poly(*L*-lactic acid), *Macromolecules*, **42**, 4739-4745, 2009.
27. Lim LT, Auras R, Rubino M, Processing technologies for poly(lactic acid), *Prog Polym Sci*, **33**, 820-852, 2008.
28. Bian J, Han L, Wang X, Wen X, Han C, Wang S, Dong L, Nonisothermal crystallization behavior and mechanical properties of poly(butylene succinate)/silica nanocomposites, *J Appl Polym Sci*, **116**, 902-912, 2010.
29. Liu TX, Mo ZS, Wang S, Zhang HF, Nonisothermal melt and cold crystallization kinetics of poly(aryl ether ether ketone ketone), *Polym Eng Sci*, **37**, 568-575, 1997.
30. Qiu ZB, Mo ZS, Yu YN, Zhang HF, Sheng SR, Song CS, Nonisothermal melt and cold crystallization kinetics of poly(aryl ether ketone ether ketone ketone), *J Appl Polym Sci*, **77**, 2865-2871, 2000.